Journal of Hydrology X 11 (2021) 100075

Contents lists available at ScienceDirect

Journal of Hydrology X

journal homepage: www.sciencedirect.com/journal/journal-of-hydrology-x

In-situ sampling for krypton-85 groundwater dating

Stéphanie Musy [a,*], Guillaume Meyzonnat [b], Florent Barbecot [b], Daniel Hunkeler [c], Jürgen Sültenfuss [d], D. Kip Solomon [e], Roland Purtschert [a]

[a] Climate and Environmental Physics and Oeschger Center for Climate Change Research, University of Bern, Sidlerstrasse 5, 3012 Bern, Switzerland
[b] GEOTOP, Université du Québec à Montréal, 201 avenue du Président-Kennedy Montréal, Québec H3C 3P8, Canada
[c] Centre d'Hydrogéologie et de Géothermie, University of Neuchâtel, Rue Emile-Argand 11, 2000 Neuchâtel, Switzerland
[d] Institut für Umweltphysik, University Bremen, Otto-Hahn-Allee 1, 28355 Bremen, Germany
[e] Department of Geology and Geophysics, University of Utah, 115 S 1460 E, Salt Lake City, UT 84112, USA

ARTICLE INFO

Keywords:
Noble gases
Tracers
Groundwater
Dating
Sampling Methodology

ABSTRACT

Krypton-85 and other radioactive noble gases are widely used for groundwater dating purposes. ^{85}Kr analysis require large volumes of water to reach the analytical requirements. Conventionally, this water is pumped to the surface to be degassed with a gas extraction system. The large pumping rate may disturb the natural flow field and requires substantial field logistics. Hence, we propose a new *in-situ* degassing method, in which membrane contactors are used to degas the groundwater directly in the well and gas is collected at the surface. This way, field work is facilitated, groundwater system disturbance is minimized, and the gas sample is collected at a specific depth. We demonstrate the tightness of the system regarding atmospheric air contamination for a collection times of 24 h, which is sufficient for both low-level counting and laser-based counting methods for ^{85}Kr. The minimal borehole diameter is 7.5 cm for the prototype presented in this research but can easily be reduced to smaller diameters. In a case study, we compare the results obtained with the new passive method with those from a conventional packer setup sampling. Additionally, ^{3}H/^{3}He samples were collected for both sampling regimes and the dating results were compared with those from ^{85}Kr. A good agreement between tracer ages is demonstrated and the age stratigraphy is consistent with the expected age distribution for a porous unconfined aquifer. In addition, our study emphasizes the differences between the age information sampled with various methods. In conclusion, we demonstrate that the new *in situ* quasi-passive method provides a more representative age stratigraphy with depth in most cases.

1. Introduction

Groundwater is an essential resource for human societies, as a source of drinking water, but also for agricultural and industrial applications. The anthropogenic stress on groundwater is increasing with the population's growth as well as a consequence of climate change. The deterioration in quality and quantity arising from these changes can be limited by a comprehensive understanding of underground flow patterns, recharge rates, and residence time distributions. These parameters are crucial to appraise the complexity of groundwater systems, especially regarding pollutants transport. Their assessment leads to more effective strategies for sustainable withdrawal.

In this context, groundwater age information is required for two purposes. Firstly, the age stratigraphy is directly linked to water quality and a key information for the estimation of the young water fraction, which is more vulnerable to anthropic contamination (Bethke and Johnson, 2008; Purtschert, 2008). Secondly, the age information is required for the calibration and validation of numerical hydrodynamic models as well as for groundwater fluxes constrain (Zuber et al., 2011).

Environmental tracers are used to characterize the groundwater travel time along the flow path because they are inherently more integrative than standard methods (i.e., artificial tracers or Darcy Law estimations). They are largely distributed near the earth's surface, and their variations are used to describe environmental processes (Cook and Böhlke, 2000). Dating tracers can be either event markers (Cook and Solomon, 1997), or accumulating in the subsurface (Darling et al., 2012), or decreasing by radioactive decay (Althaus et al., 2009; Collon, Kutschera and Lu, 2004; Lu et al., 2014; Tomonaga et al., 2017). Because different tracers behave differently in case of mixing, additional information is provided when they are applied simultaneously (Kagabu et al.,

* Corresponding author.
E-mail address: stephanie.musy@climate.unibe.ch (S. Musy).

https://doi.org/10.1016/j.hydroa.2021.100075
Received 13 November 2020; Received in revised form 7 February 2021; Accepted 10 February 2021
Available online 18 February 2021

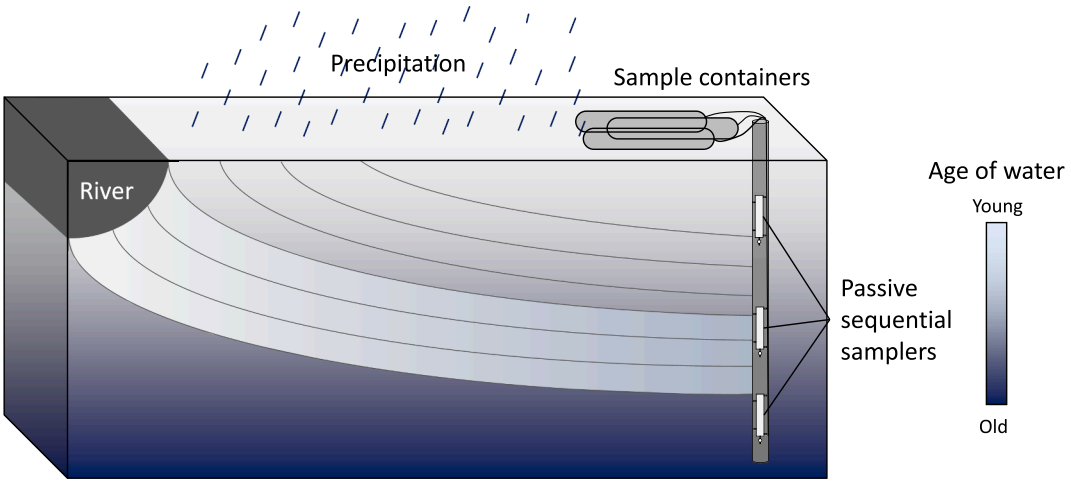

Fig. 1. Depth-dependent sampling in the context of aging with depth in a uniform porous media with an infiltrating river.

2017; McCallum, Cook and Simmons, 2015). Among environmental tracers, noble gas radionuclides are especially interesting because of their inertness and thus, their insensitivity to degradation or retardation processes due to chemical reactions. However, their low abundances in the environment require relatively large volumes of water for analysis.

For this purpose, groundwater degassing in the field is conventionally achieved through either a vacuum extraction chamber or membrane contactors. The water is pumped from the well into the apparatus by a submersible pump and discharged after gas extraction (Gerber, 2012; Ohta et al., 2009; Purtschert and Yokochi, 2013; Yokochi, 2016). These traditional pumping and degassing setups are logistically challenging, and impractical for very low productivity wells with very long sampling times. In addition, active pumping may induce drawdown that disturbs the natural age stratification and, in some cases could even lead to infiltration of gas from the vadose zone.

As an alternative, we propose an approach in which the water is degassed directly in the well for krypton-85 groundwater dating. Membrane modules are placed at a defined depth in the wellbore and left in place for several hours during which the gas is autonomously extracted, transferred to the surface, and collected in sampling vessels. This method offers several advantages. Firstly, no gas pump, or compressor is required in the field if the gas is extracted in pre-evacuated gas vessels. Secondly, the risk for atmospheric air contamination during prolonged sampling times is minimal since most connections and the membranes are immersed under water. Finally, several samplers can simultaneously be placed at different depths allowing to establish groundwater age profiles without using expensive packers systems (Fig. 1). This way, the sampling procedure is facilitated while the disturbance of the natural flow field is minimized. Its use is especially interesting in porous aquifers with dominant horizontal flow. The application in fractured aquifers is more complex because of localized groundwater inflows that may induce ambient vertical flow in the wellbore. However, if these fluxes are quantified, the method allows for the deconvolution of the activities, and the dating of the water inflows (Meyzonnat et al., 2018).

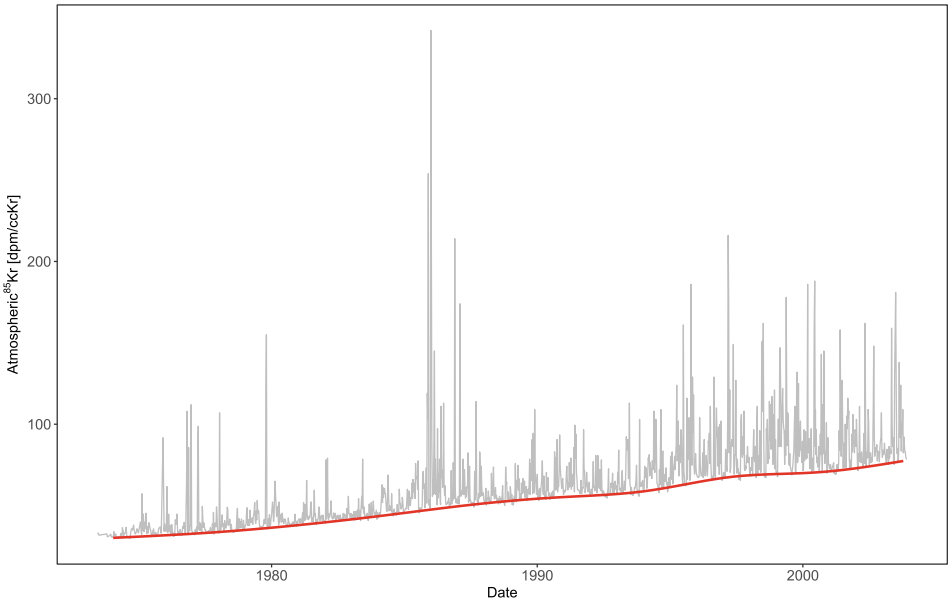

Fig. 2. Atmospheric ^{85}Kr activities [dpm/cc$_{Kr}$] weekly measured in air in Freiburg by the German Federal Office for Radiation Protection at Freiburg (Source: Bollhöfer et al. 2019) .The red line is the baseline calculated with a running average of minima over 15 weeks. The peaks represent pulsed releases from reprocessing plants mainly in La Hague (France). (For interpretation of the references to colour in this figure legend, the reader is referred to the web version of this article).

2. Method

2.1. ^{85}Kr groundwater dating

Krypton-85 (^{85}Kr) is a noble gas radionuclide with a half-life of 10.74 years used to date young groundwater in the age range from 5 to 50 years (Purtschert, 2008; Singh and Chen, 2014). This radioisotope is naturally produced in the earth atmosphere by cosmic rays ($^{84}Kr(n,\gamma)^{85}Kr$), and fission reactions in the lithosphere. However, the major part of ^{85}Kr is anthropogenic as it is produced in nuclear reactors by fission of uranium and plutonium, and released during reprocessing of nuclear spent fuel (Ahlswede et al., 2013; Bollhöfer et al., 2019). This results in a steadily increasing activity concentration in the atmosphere since 1950 s up to about 80 dpm/cc_{Kr} (decay per minute and cm^3_{STP} krypton) in 2019 (Fig. 2). In the proximity of re-processing plants (in Europe: mainly around La Hague, in France), the atmospheric ^{85}Kr activity concentration varies temporally due to pulsed releases (Bollhöfer et al., 2019). An interhemispheric exchange time of roughly one year, and the fact that all reprocessing plants are located in the northern hemisphere, lead to a smoother and 15% lower ^{85}Kr activity course in the southern hemisphere (Ahlswede et al., 2013; Lu et al., 2014; Kersting et al., 2020).

Once precipitation reaches the groundwater table, gas and ^{85}Kr exchange with the atmosphere is blocked. The ^{85}Kr activity decreases along the groundwater flow path due to radioactive decay. Mixing at variable scales as well as diffusion/dispersion processes lead to a distribution of residence times rather than a single age (Suckow 2014). The probability distribution of ages $g(t)$ (Małoszewski and Zuber, 1982; Suckow, 2014) is commonly described by simple analytical functions. These are combined with the input tracer concentration $C_{in}(t')$ [dpm/cc_{Kr}] at recharge time t' in the convolution integral (Equation (1))

$$C_{out}(t) = \int_{-\infty}^{t} C_{in}(t') \cdot g(,t-t') \cdot e^{-\lambda_{85}(t-t')} dt' \quad (1)$$

$C_{out}(t)$ [dpm/cc_{Kr}] is the concentration at observation time t [yr], and λ_{85} [yr^{-1}] is the ^{85}Kr decay constant (6.4×10^{-2}/yr). The mean residence time τ, corresponding to the weighted average value of all idealized ages (t-t'), is one of the model parameters describing the probability distribution $g(t)$. τ can be determined by an optimisation routine once the functional form of $g(t)$ has been specified.

The dating method is based on the measurement of the specific ^{85}Kr activity per volume of total krypton. The concentration of stable krypton isotopes in the atmosphere remains constant at 1.099 ppm(v) (Aoki and Makide, 2005). Transitions between liquid and gas phase, i.e. gas dissolution and degassing, fractionates the $^{85}Kr/Kr$ ratio to <1% for most realistic scenarios (Purtschert, 2008). Dating results are therefore not sensitive to recharge temperatures or excess air (Heaton and Vogel, 1981), nor to partial degassing prior or during sampling. This is a big advantage compared to other tracers based on absolute concentrations of dissolved gasses.

The composition of gas dissolved in water is determined by solubility, which itself depends on temperature and salinity, and the partial pressure of the gas in the atmosphere. The concentration of krypton in air equilibrated water (A.E.W) at sea level and for a recharge temperature of 10 °C is 9.2×10^{-2} µL/L of water. For these conditions, the dissolved gas fraction is 3.93 ppm(v). The minimal amount of krypton required for ^{85}Kr analyses is 1–2 µL for both Low-Level Decay Counting (LLC) and Atom Trap Trace Analysis (ATTA) analyses (Loosli and Purtschert, 2005; Lu et al., 2014; Zappala et al., 2017). Considering a degassing efficiency of ~50%, losses during gas purification, and gas transfer into the detection system of another 50% loss, leads to a minimal amount of groundwater of ~50–200 L that needs to be processed in the field.

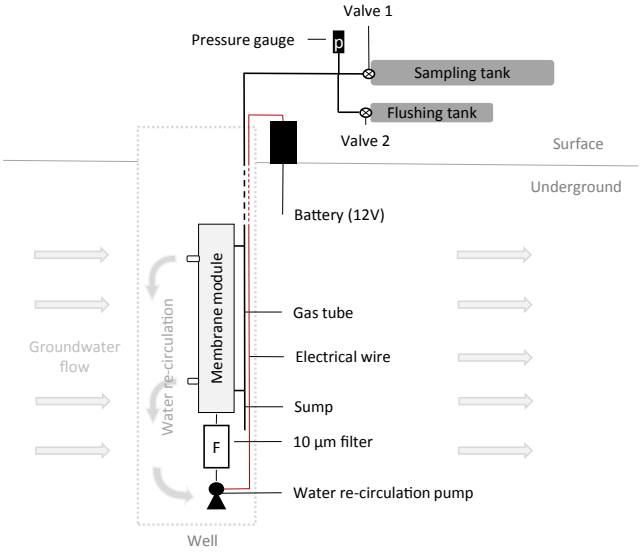

Fig. 3. Degassing setup. The water is circulated through the membrane module between the two outlets of the contactor to the water pump.

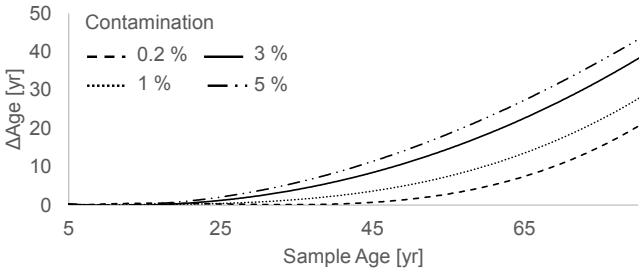

Fig. 4. Age error (ΔAge) induced by modern air contamination as function of the piston flow age for different contamination percentage. We assume a modern activity of 80 dpm/cc_{Kr}.

2.2. Experimental setup

We present a new sampling system in which small membrane contactors (cells) are inserted directly in the well and the gas is collected at the surface. Fig. 3 illustrates the setup with one degassing unit, composed of a membrane contactor with an internal surface of 2500 cm^2 (PDMSXA-2500; PermSelect®), a water filter, a small water pump (DM212VS; Dynamax Pump Series®) and a sump. The water is locally recirculated through the membrane with a flow rate of 1 L/min, which brings enough water in contact with the membrane within a sampling time of 24 h, while only minimally disturbing the natural flow field (quasi-passive sampling). The 12 V small water pump is powered by a car battery at the surface. The module is connected by a ¼-inch copper or plastic (PP or PE) tubing to a pre-evacuated sampling tank (20 L) at the surface. The volume of the gas line is ~ 30 cm^3/m. To avoid clogging of the membrane, the water is cleaned by a 10 µm filter unit. The pressure gradient between both sides of the membrane drives the gas through the membrane and to the sampling bottle. The sample pressure in the tank is continuously monitored during the experiment by a pressure gauge at the surface. The hydrophobic membrane is permeable to some degree to water vapor and a sump (~10 cm^3) is included in the setup to avoid clogging of the gas line by water. The diameter of our prototype sampler, without the plastic inserts, is 2.5 cm. The whole prototype setup fits in a 7.5 cm borehole, but future versions will fit in a 5 cm (2 in.) wellbore. Before the sampling starts, the gas lines and connections are evacuated to avoid any contamination by atmospheric air. This can be done by a second pre-evacuated, tank (e.g. 10 L) connected to the degassing line

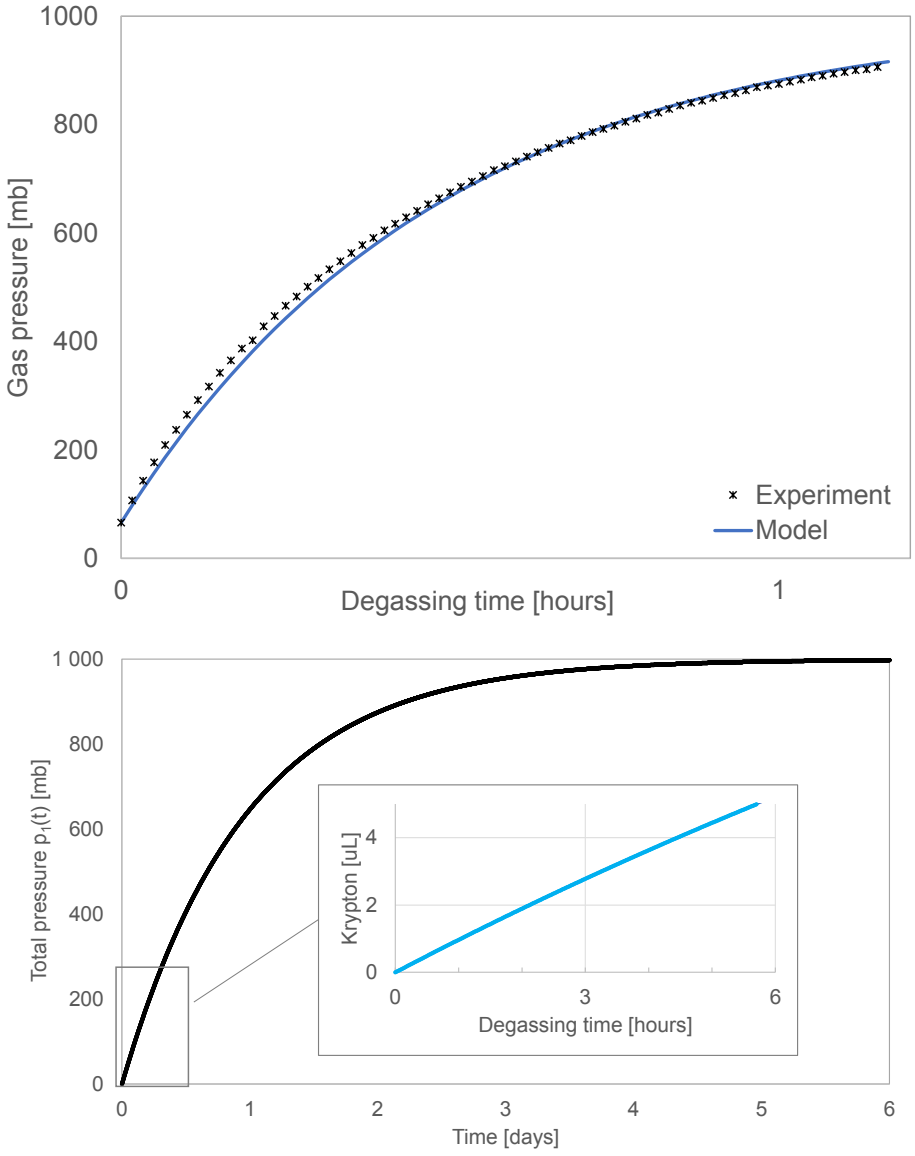

Fig. 5. a) Equilibration experiment (crosses) compared to the fitted values with $K_{air} = 5.3 \times 10^{-7}$ cm^2/s, V = 420 cm^3; b) Pressure increase in a 20 L tank and corresponding volume of krypton sampled assuming A.E.W at 10 °C and a processing efficiency of 50%.

(which has a volume of 0.3 L/10 m.). Another option for flushing the line is to connect a vacuum pump to valve 2.

For the determination of age-depth profiles, several degassing units are aligned in a serial configuration and individually connected to pre-evacuated flushing and sampling tanks. For a 10 L flushing tank (evacuated < 0.1 mb), and a tube length of 10 m, the residual pressure in the line is 30 mb. For a 5 L gas sample this residual gas volume of ~ 9 cc/10 m corresponds to 0.2% air contamination or ~ 0.14 dpm/cc$_{Kr}$ (Fig. 4). This is below the analytical uncertainty of 0.2–0.5 dpm/cc$_{Kr}$ and could only become relevant for old waters with ^{85}Kr activity levels <2 dpm/cc$_{Kr}$. After closing the flushing tanks, the sampling tanks are opened. The setup remains in the well for at least 24 h during which about 5–10 L of gas are collected from A.E.W. After gas collection the pressure in the tank is recorded, the sample bottle is closed, and the line is withdrawn.

The principle of gas sampling based on permeation through a membrane has been previously described and tested by Gardner and Solomon (2009) for stable noble gases and ^{3}H/^{3}He dating. The required total dissolved gas pressure (TDGP) at sampling depth is either measured by a separate probe in the borehole or preserved by closing the gas vial *in situ* and measured afterwards in the laboratory. In contrast, our sampling method does not require the knowledge of the TDGP because the age is determined by the activity ratio ^{85}Kr/Kr.

2.3. Degassing principles

A gas extraction system for groundwater dating purposes must (i) be leak-tight, to avoid sample contamination by modern air (Fig. 4) (Lu, 2014; Purtschert and Yokochi, 2013) (ii) have a high extraction yield to minimize the volume of water required and the extraction time, and (iii) be sufficiently robust, light, and portable for field work. The concepts of our approach are discussed in detail in the following sections.

2.3.1. Phase separation by membranes

A membrane is a selective layer of material for a substance passing through it. The gas permeation process is composed of consecutive gas solution on the high pressure side, diffusion through the membrane and evaporation on the low pressure side (Sanders et al., 2013) (Fig. A.1 in Appendix). The dissolution and evaporation processes conform to Henry's Law while diffusion follows Fick's first law (Ahsan and Hussain, 2016; Zhang and Cloud, 2006).

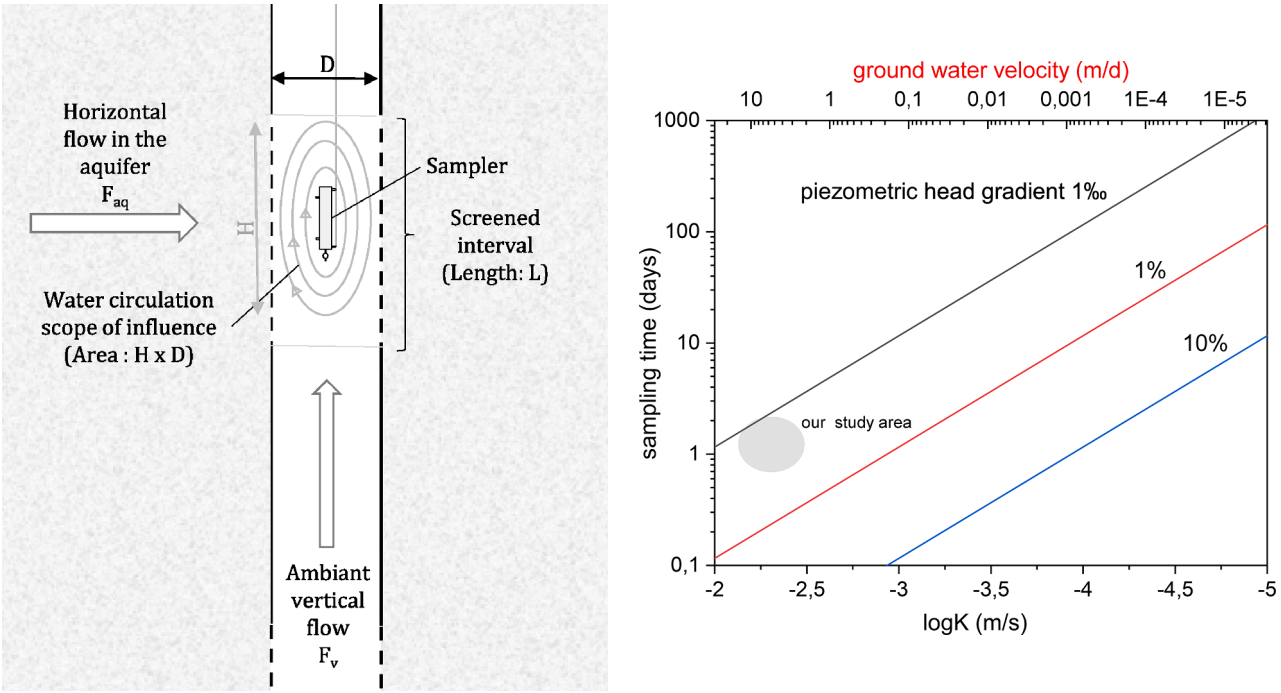

Fig. 6. a) Scheme of water circulation in the aquifer and in the borehole b) Sampling time as function of the aquifer conductivity and piezometric head gradient. For the graph, the following parameters were assumed: minimal sample volume $V_w = 100$ L, borehole diameter D = 10 cm, range H of circulation pump: 1 m, $A_{HD} = 0.1$ m^2 (Equation (5)). The water flow velocity (upper x-axis) refers to dh/dz = 1% and a porosity of 30%. For a head gradient of 1% aquifers with K $<10^{-4}$ m/s can be sampled within days. Lower conductivities require active pumping in order to increase the head gradient (e.g. to 10%). In the reference aquifer presented in the following, a sampling time of ~1 day is sufficient (shaded area).

The pressure increase on the gas side (shell side) of the membrane, which includes the volume of the gas lines and the sampling container V [cm^3] (Fig. 3), is linked to the gas flow rate through the membrane (i.e. the degassing yield). The resulting pressure increase as function of time $p_1(t)$ [mb] is described by Equation (2) (and derived in Equations (A.1) – (A.4) in Appendix), where p_0 [mb] is the total dissolved gas pressure (TDGP), K [cm^2/s] is the diffusion coefficient of gas through the membrane, l [cm] is the membrane thickness, and A [cm^2] is the membrane surface area (Gardner and Solomon, 2009). Note that $p_1(t=0) \cong 0\ mb$.

$$p_1(t) = p_0 \cdot (1 - e^{-\frac{KA}{lV}t}) \tag{2}$$

2.3.2. Extraction efficiency

The extraction efficiency is defined as the proportion of gas sampled (gas yield or flux) in relation to the dissolved gas content in water, which is maintained constant throughout the experiment thanks to water renewal (Equation (3)).

$$Efficiency = \frac{Gas\ flux\ through\ the\ membrane\ \left[\frac{cc}{min}\right]}{Water\ flux\ \left[\frac{L_w}{min}\right] \cdot Gas\ content\ \left[\frac{cc}{L_w}\right]} \tag{3}$$

The efficiency is determined by membrane characteristics (surface area, thickness, material, gas dissolution and diffusion coefficients), but also by the solubility and diffusivity of the gas in the water. It further depends on the partial pressure of the gas in the water, and decreases with decreasing contact time with the membrane, which is inversely related to the water flow rate. The efficiency drops from 80% to 40% if the water flow rate increases from 0.3 L/min to 2 L/min (Fig. B.1 in Appendix). If the gas is collected in a pre-evacuated container, the pressure gradient between both sides of the membrane, and thus the efficiency, decreases over time.

2.3.3. Head loss along the gas tube

The pressure loss along the gas lines between the membranes (in the borehole) and the sample container (at the surface) can be described by the Darcy–Weisbach equation (Brown, 2000) simplified for laminar flow in a circular pipe (Equation (4)).

$$\frac{\Delta P_f}{L} = \frac{128}{\pi} \frac{\mu \cdot Q_t}{D^4} \tag{4}$$

where ΔP_f [mb] is the pressure loss in a tube with a length L [m], μ [Pa·s] is the dynamic viscosity of the fluid, i.e. 1.78×10^{-5} Pa·s for air at 10 °C (White, 1988), Q_t [m^3/s] is the volumetric flow rate, and D [m] is the tube diameter. A typical gas flux Q_t of 0.4 cc/s is calculated assuming a water flowrate of 1 L/min, a gas content of 23 cc/L, and a degassing efficiency of 50%. For an inner diameter of ¼ inches, and a 50 m long tube, the pressure loss is in the order of 10^{-2} mb. This is negligible in comparison to the driving pressure difference in the order of several hundreds of mb.

2.4. Performance and testing

2.4.1. Equilibration experiment

A water degassing experiment was performed in the laboratory to determine the diffusion coefficient for air through the membrane, K_{air} [cm^2/s]. For this purpose, tap water (i.e., A.E.W, constantly renewed) is circulated through the membrane with a flow rate of 1 L/min and degassed into a volume of ~ 400 cm^3.The pressure increase is recorded as function of time with a pressure gauge (Fig. 5a). These experimental data are then fitted with Equation (2) to extrapolate K_{air}. The resulting diffusion coefficient for air, $K_{air} = 5.3 \times 10^{-7}$ cm^2/s, is similar to the diffusion coefficient of argon and krypton through silicone concluded by Gardner and Solomon (2009).Therefore, we use this value to assess the krypton extraction yield in the following.

As discussed earlier, the targeted amount of krypton that needs to be extracted from the water is 2–4 µL (with 50% losses during gas purification and transfers to the counting system). Assuming A.E.W at 10 °C, and thus a krypton concentration of 3.93 ppm(v), the collection time is

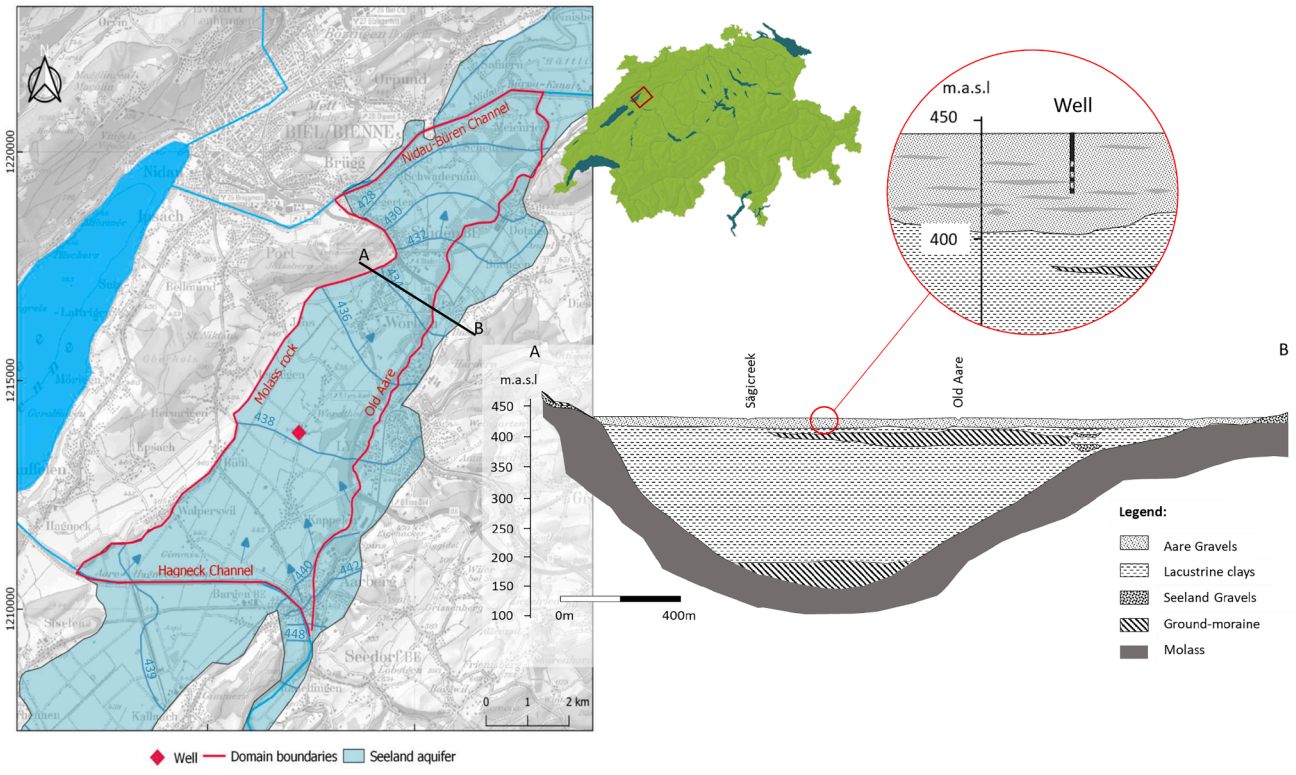

Fig. 7. Field site in the North-Seeland aquifer in Switzerland, and cross section of the area (modified from Biaggi et al., 2004). The well location is projected. The Aare gravel contains silty lenses/layers represented by the grey shapes.

5 h for 4 µL in a 20 L tank (Equation (2) and Fig. 5b). An equilibration time of 24 h should therefore be sufficient for most scenarios and conditions (partly degassed water, higher recharge elevation or temperature).

This degassing experiment allowed to assess the air degassing efficiency of our samplers. For this purpose, the gas volume sampled is compared with the total gas dissolved in the water circulating around the membrane. The median extraction efficiency observed is 21%, for a final sample pressure of 500 mb, i.e., 10 L of gas in a 20 L sample bottle and A.E.W at 10 °C circulated at 1 L/min.

2.4.2. Leak test

The leak rate in operation mode is evaluated by introducing the sampler in stagnant water and degassing it in a known sampling volume of 25 cm^3. The pressure increase is recorded as a function of time by a pressure gauge. After a few minutes, the water in contact with the membrane is completely degassed and the following pressure increase is interpreted as a maximal leak rate. The experiment was carried out for 5 days. The average leak rate was 0.27 mb/hour, corresponding to a gas flux of 1.1×10^{-4} cc/min. In comparison with the mean degassing rate of 5 cc/min for A.E.W, for a pump rate of 1 L/min and a degassing efficiency of 20%, this leak rate corresponds to an air contamination of 0.03‰ what is negligible in relation to the analytical uncertainty of ^{85}Kr analyses (Zappala et al., 2017) and the methodological dating errors.

2.5. Applicability and limitations of the method

A constrain of the method arises from the minimum volume of water that needs to be degassed in the borehole, and therefore needs to be in contact with the degassing unit within a reasonable sampling time. With other words: the natural groundwater flow through the borehole within the targeted sampling time t_s must reach at least the minimum water sample volume of 100 L (V_w) (Equation (5)).

$$t_s = \frac{V_w}{F_{BH}} = \frac{V_w}{v_{Darcy} \cdot A_{HD}} = \frac{V_w}{K \cdot \frac{dh}{dx} \cdot A_{HD}} \quad (5)$$

where F_{BH} $[m^3/d]$ is the water flow rate through the effective borehole cross section A_{HD} $[m^2]$ (Fig. 6a), v_{Darcy} $[m/d]$ is the Darcy velocity in the aquifer as function of the aquifer conductivity K $[m/s]$ and piezometric head gradient dh/dx (Fig. 6b) (Raja Sekhar and Sano, 2000). In the case where the natural flowrate is too low to allow water renewal within a reasonable sampling time, recirculation of water that was already partly degassed would eventually lead to a standstill of the gas flow (Harrington, Cook and Robinson, 2000).

A potentially limiting factor for any passive sampling method are ambient vertical flows (AVF) in presence of a vertical head gradient along the borehole (Corcho Alvarado, Barbecot and Purtschert, 2009; McMillan et al., 2014). The acceptable threshold for upwelling flow depends on the context, the natural age stratigraphy in the aquifer and the distance that separates the screens or the inflows. Note that this type of limitation is common to all passive sampling methods and generally, it must be clear that almost no vertical flow is acceptable with these methods. AVF are especially common in fractured rocks because of the natural difference in hydraulic heads. In this case, a pump might be placed at the top in order to control the flow direction and intensity in the wellbore. The intensity and location of water inflows in the borehole need then to be quantified by suitable borehole logging techniques (Meyzonnat et al., 2018). The effect of AVF can be reduced by separating depth sections with flow barriers (very simple packers or disks) that impede water exchange between distinct depth levels.

Special attention must be paid in case of high dissolved gas contents (e.g., CO_2, CH_4), which will result in a faster increase of pressure in the sample tank. The size of the tank needs to be adjusted accordingly. In addition, suspended matter in the water may clog the filter and the membrane. In this case, a series of filters with increasing mesh should be added.

Table 1
Analytical results of ^{85}Kr and ^{3}H/^{3}He measurements, and derived Piston-Flow ages. Passively taken samples are in shaded boxes. Passive $^{3}He_{trit}$ values were calculated for degassing (i) at recharge – (ii) just before sampling.

Mean Depth	Conventional		Passive		Passive	
	^{85}Kr dating					
	April 2019		April 2019		December 2019	
	^{85}Kr [dpm/cc$_{Kr}$]	Age [yr]	^{85}Kr [dpm/cc$_{Kr}$]	Age [yr]	^{85}Kr [dpm/cc$_{Kr}$]	Age [yr]
9	65 ± 2.5	6 ± 0.4	52 ± 1.9	7 ± 0.5	66 ± 3.4	6 ± 0.4
15	63 ± 2.0	6 ± 0.4	54 ± 3.9	7 ± 0.7	57 ± 1.8	7 ± 0.4
22	50 ± 4.3	8 ± 0.8	41 ± 4.2	11 ± 1.3	43 ± 1.9	11 ± 0.7
	^{3}H /$^{3}He_{trit}$ dating					
	April 2019			December 2019		
	^{3}H [TU]* ± 1.1	$^{3}He_{trit}$ [TU]* ± 0.4	^{3}H/^{3}He Age [yr]	$^{3}He_{trit,c}$ [TU]* ± 0.5	^{3}H/^{3}He Age [yr]	
9	11	6	8 ± 0.8	- 0.7	-1 ± 0.7	
15	10	5	7 ± 0.8	11 – 10	13 – 12 ± 1	
22	8	19	21 ± 1.7	20 – 18	22 – 20 ± 1.7	

*4.0193 10^{-14} cc/g = 1 TU

*4.0193 10^{-14} cc/g = 1 TU.

3. Case study in the Seeland aquifer (CH): comparison with conventional sampling and ^{3}H/^{3}He ages

3.1. Field site

The Seeland Region is situated in the Northwestern part of Switzerland between the city of Bern and the lake Biel (Fig. 7). In this area, the successive avulsions of meandering Aare River led to a variable lithology that range from well-sorted gravels to clay. Our observation well is situated in the area of Kappelen, where these alluvial gravel deposits are up to 50 m thick. The basement rock is the Tertiary Molasse of the Swiss Plateau covered by ground-moraines and glacio-lacustrine clay sediments up to 200 m deep (Fig. 7). Until the 19th century, this area was a floodplain of the Aare River and its exploitation for human activities was limited. Later, the area was drained by a wide series of hydrological undertakings (e.g., channelization of the rivers) to lower the water table and to protect the area from flooding. Nowadays, the Seeland region is one of the most productive agricultural areas in Switzerland (Baillieux et al., 2014; Biaggi et al., 2004; Gobat, 2015; Kozel, 1992).

Hydrogeological boundaries are delimiting our area (Fig. 7). First, the Seeland aquifer is separated between the northern and southern part by the Hagneck-channel, which acts as a water divide caused by the strong infiltration of channel water (Baillieux et al., 2014). In this case,

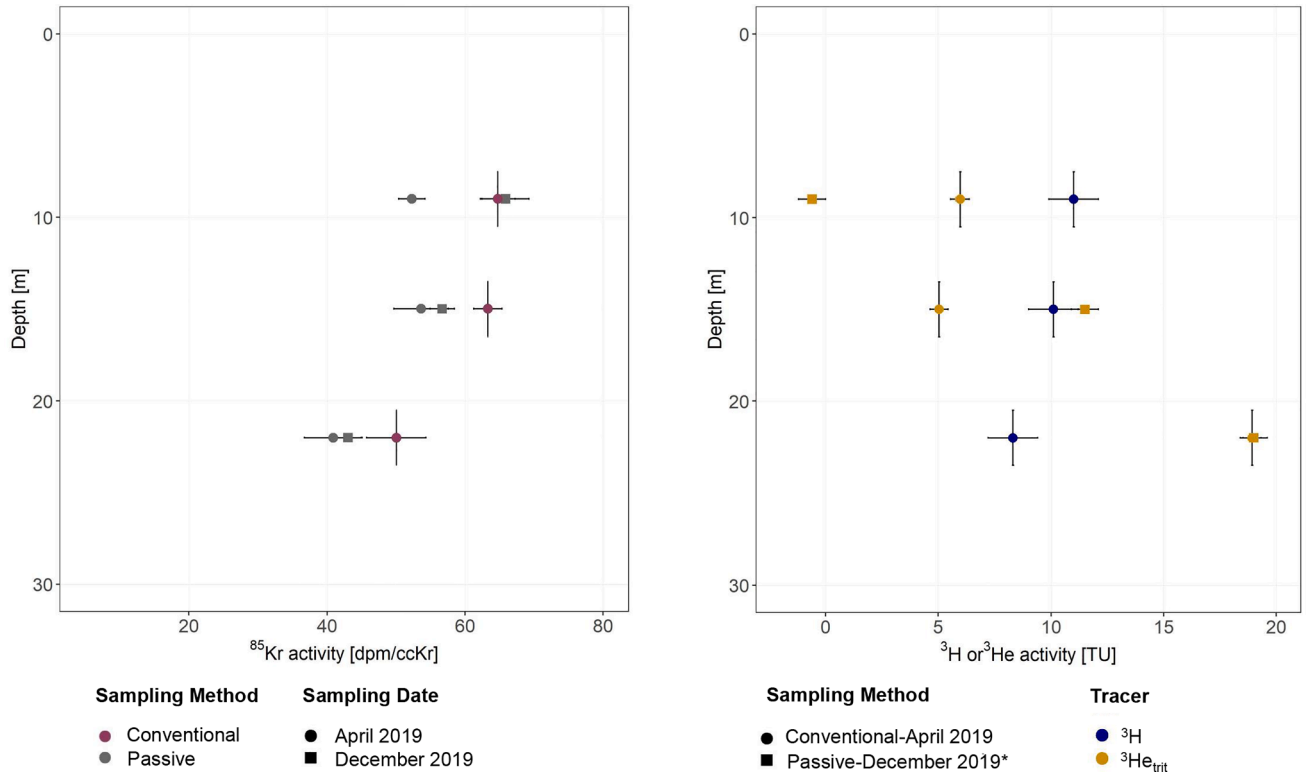

Fig. 8. ^{85}Kr activity concentration, ^{3}H, and $^{3}He_{trit}$ profiles with depth. The passive $^{3}He_{trit}$ values are an average of the two degassing scenarios discussed before.

Table 2
Concentrations of noble gases for conventional and passive sampling. A solubility equilibrium degassing correction was applied for samples with total dissolved gas pressures (TDGP) < 1. V_g and f_{He} are the volume of the gas phase and the fraction of ^{3}He remaining in solution after degassing (after Visser, Broers and Bierkens (2007)).

	Depth [m]	R/R_a [–]	He[a] [cm^3_{STP}/g] $\times 10^{-8}$	Ne[b] [cm^3_{STP}/g] $\times 10^{-7}$	$\Delta Ne^{¥}$ [%]	$\Delta He^{¥}$ [%]	$^4He^{¥}_{atm}$ [cm^3_{STP}/g] $\times 10^{-8}$	$^3He^{¥}_{atm}$ [cm^3_{STP}/g] $\times 10^{-14}$	TDGP [atm]	V_g [cm^3_g/cm^3_w] $\times 10^{-4}$	f_{He}
Conven-tional	9	1.18	5.2	2.2	13.3	16.5	5.22	7.13			
	15	1.14	5.3	2.2	14.3	18.2	5.27	7.2			
	22	1.58	5.4	2.2	13.7	19.9	5.24	7.15			
									1.5		
Passive	9	0.97	6.2	2.8	48.0	40.0	7.15	9.43	0.85	4.8	0.95
	15	1.4	4.1	1.9	−2.0	−7.8	4.37	5.71	0.95	6.8	0.99
	22	1.6	5.0	2.2	17.5	12.5	5.45	7.16			

[a] ±0.05; [b] ±0.02; [¥] for a recharge elevation of 500 m and a MAAT of 13 °C.

we are interested in the northern part where the water flows towards the north-eastern direction to the Nidau-Büren channel. The Old Aare river is the south-eastern hydrogeological barrier. The north-western boundary is the outcropping of the Tertiary Molasse (Cochand et al., 2019; Gobat, 2015).

In this area, groundwater recharge occurs by two main processes. Firstly, infiltration of local precipitation, that percolates through soil and thus, drains the minerals and the pesticides applied on the farmlands. The recharge elevation is thus 500–550 m and the mean annual air temperature (MAAT) is ~13 °C. The second recharge process is infiltration from the Hagneck-channel as well as the Old Aare streambed. In contrast to recharge from local precipitation, this water is less mineralized and depleted in heavy isotopes since the catchment area of the river Aare is at higher altitude in the Alps. These two main recharge components are mixed in the aquifer. Previous studies suggested a proportion of Aare river water of up to 50% at our sampling well (Gobat, 2015)

The aquifer conductivity and hydraulic head gradient were estimated to be in the order of 10^{-2} m/s and 2‰ (Gobat, 2015; Kozel, 1992). This results in a water flow velocity of ~10 m/d for a porosity of 20–30%.

The sampling location in Kappelen is a test well with a depth of 25 m and a diameter of 10 cm (Fig. 7). The lithology is mainly composed of permeable sandy gravels (Aare gravels) alternating with an increasing proportion of silty layers with depth (Gobat, 2015). In the borehole casing, three screened intervals are located at 7.5–10.5 m, 14–17 m, and 20.8–23.8 m. Special attention was paid at the time of drilling to avoid leakage between the screened levels via the borehole filling around the casing.

3.2. Sampling and analytical methods

The field site in Kappelen was chosen because of its relatively simple hydrology and the possibility for multi-level sampling. Two field campaigns were conducted in April and December 2019 for ^{85}Kr, tritium, stables isotopes of the water molecule, and stable noble gases. The main objectives of this case study were (i) to compare ^{85}Kr dating results obtained by passive and active sampling and (ii) to further assess and interpret these results by means of additional dating tracers such as ^{3}H/^{3}He.

In April 2019, three passive degassing units were left in the well for 24 h at the center of each screen (9, 15, and 22 m). The well was undisturbed (i.e., not flushed) prior to sampling. An active sampling was carried out immediately after removing the passive samplers from the well. For this purpose, the three screened intervals were successively isolated by packers, flushed with a submersible pump (MP1; Grundfos®), and sampled for ^{85}Kr using a vacuum extraction system (Purtschert and Yokochi, 2013). 600 L of water from each level were degassed with a flow rate of 24 L/min. These samples are denoted “conventional” in the following. Additional samples for ^{3}H, and δ^{18}O and δ^2H were collected, and stable noble gasses samples were taken in pinched off copper tubes (Beyerle et al., 2000).

In December 2019, passive ^{85}Kr sampling was repeated at the same three levels. Directly afterwards (without purging the well), ^{3}He as well as stable noble gases were collected using the equilibration samplers developed by Gardner and Solomon (2009). These “passive” noble gas samples and ^{3}H values from April were used for ^{3}H/^{3}He dating. The well was undisturbed for more than 6 months before this sampling campaign.

The ^{85}Kr activities were measured by LLC (Purtschert and Yokochi, 2013) in the deep laboratory from the University of Bern. Stable isotopes of the water molecule were also measured at the University of Bern (Huber and Leuenberger, 2005). Stable noble gases were measured at the Institute of Environmental Physics of the University of Bremen (Sültenfuß, Roether and Rhein, 2009) for the conventional samples, resp. at the Department of Geology and Geophysics of the University of Utah for the passive samples (https://noblegaslab.utah.edu). ^{3}He, ^{4}He,

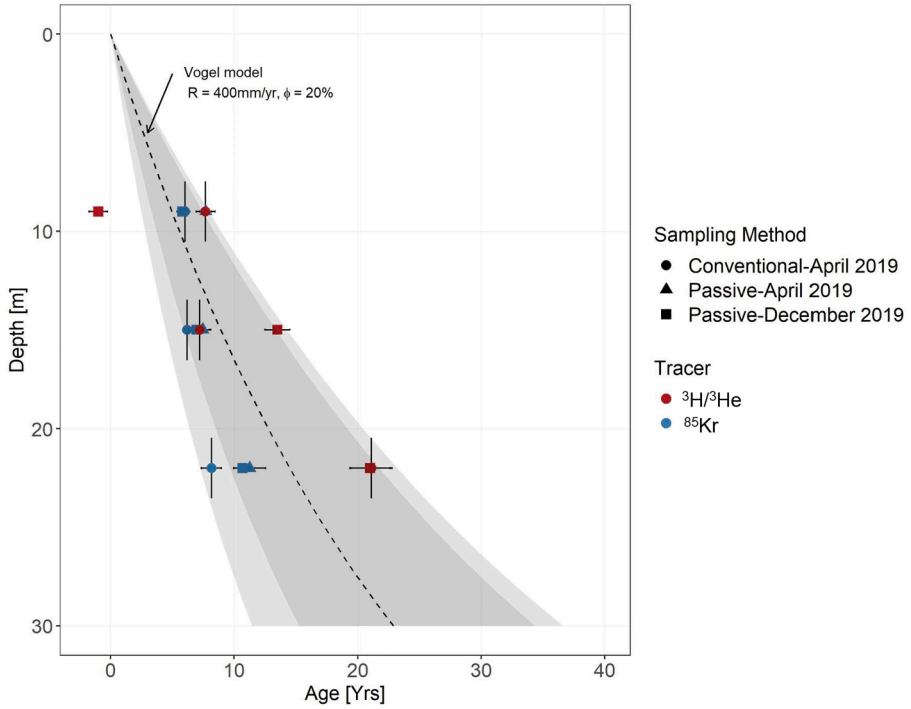

Fig. 9. Age profile with depth for ^{85}Kr and ^{3}H/^{3}He ages with different methods. The dotted line represents the Vogel Model assuming an aquifer thickness of 50 m, a porosity of 20% and a recharge rate of 400 mm/yr; the grey areas show the range of Vogel model for recharge rates between 250 and 600 mm/yr and porosities between 10% and 30%. The passive ^{3}H/^{3}He age are an average of the two degassing scenarios discussed before.

Table 3
Stable isotopes of the water molecule.

	April 2019		December 2019	
	δ^{18}O **(VSMOW) ± 0.1	δ^{2}H (VSMOW) ± 0.5	δ^{18}O (VSMOW) ± 0.1	δ^{2}H (VSMOW) ± 0.5
9	−11.2	−81.3	−11.8	−83.2
15	−11.2	−82.2	−11.8	−83.1
22	−11.1	−80.7	−11.9	−83.6

**(VSMOW: Vienna Standard Mean Ocean Water).

and Ne measurements are used to calculate the ^{3}H/^{3}He ages.

3.3. Results

Table 1 shows the ^{85}Kr and ^{3}H/^{3}He$_{trit}$ concentrations with corresponding piston flow ages. ^{85}Kr activity concentrations decrease with depth from 65 dpm/cc$_{Kr}$ to 50 dpm/cc$_{Kr}$ for conventional sampling (Fig. 8). Tritium values range from 11 TU to 8 TU with a decreasing trend with depth. ^{85}Kr and ^{3}H both suggest the presence of young water (<60 years) at all depths. The samples collected with the new passive samplers for ^{85}Kr show a very similar pattern than the conventional samples but with values systematically ~10 dpm/cc$_{Kr}$ lower. This difference between the passive and the conventional activities is discussed in Section 3.4. For the two deeper levels, the repeated ^{85}Kr measurements in April and December agree. The temporal variation observed for the shallow level may indicate changes of the proportion of young water in an active recharge system.

Noble gas samples were collected with pinched off copper tubes in parallel to ^{85}Kr sampling (April 2019) from intervals separated by packers. These samples reveal increasing ^{3}He/^{4}He ratios (R) expressed as relative to the atmospheric ^{3}He/^{4}He ratio (R$_a$) (Table 2). Excess air (EA), denoted as Ne excess relative to the solubility equilibrium concentration (ΔNe [%]), is similar for all levels (13–14%). In contrast, noble gas data collected with the passive samplers in December 2019 (just after passive ^{85}Kr sampling) show larger scatter in R/R$_a$, △Ne values, and total dissolved gas pressures (TDGP) with even negative values (Table 2). These variations are likely related to the passive sampling regime. A better understanding of the underlying processes is required before deriving ^{3}H/^{3}He ages from these data. This is discussed in the following.

For the two deeper passive samples, TDGP below 1 atm indicates the occurrence of degassing. For the calculations of ^{3}H/^{3}He ages, a ^{3}He degassing correction was applied. For this purpose, gas loss was estimated based on the deficit of ^{4}He measured in relation to ^{4}He at solubility equilibrium (^{4}He$_{Eq}$) plus ^{4}He from excess air (^{4}He$_{EA}$, estimated from △Ne), and assuming an atmospheric Ne/He ratio (unfractionated EA). This is a modified version of the correction method proposed by Visser, Broers and Bierkens (2007), where EA was neglected. ^{3}He$_{trit}$ is then calculated under the assumptions that (i) degassing occurred at recharge (no loss of ^{3}He$_{trit}$) and (ii) degassing occurred shortly prior or during sampling (with ^{3}He$_{trit}$ loss) (Equation (6)).

$$(i)\ {}^{3}He_{trit,c} = {}^{3}He_{m} - f_{He}\cdot He_{atm} \quad (ii)\ {}^{3}He_{trit,c} = \frac{{}^{3}He_{m}}{f_{He}} - He_{atm} \tag{6}$$

f$_{He}$ is the remaining fraction of He after degassing (Table 2), ^{3}He$_m$ is the measured concentration and ^{3}He$_{atm}$ is the atmospheric concentration before degassing (^{3}He$_{Eq}$+^{3}He$_{EA}$). Since the point in time of degassing is unknown, both corrections were applied leading to a

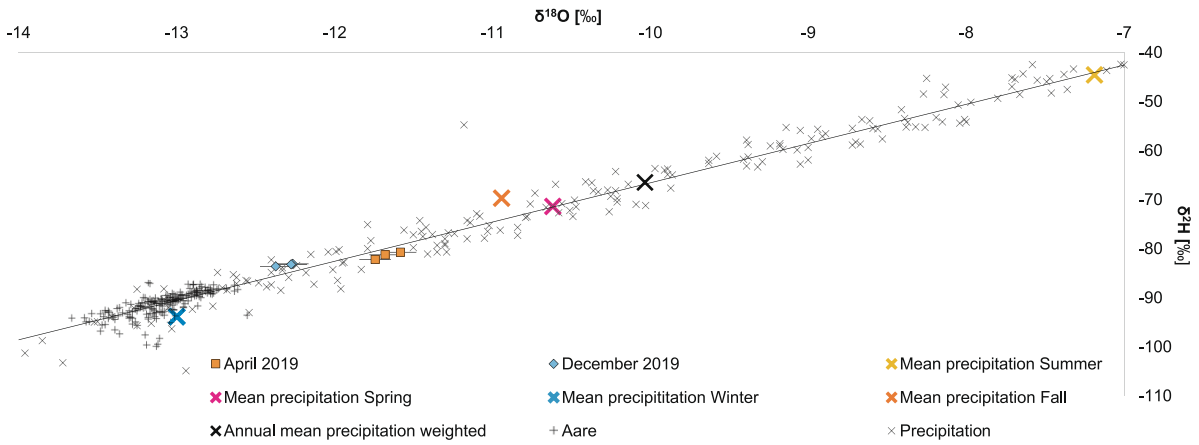

Fig. 10. Stable isotopes of the well in Kappelen (Switzerland), signature in precipitation monthly averaged measured in Bern and Aare water monthly averaged measured in Thun (Source: Global Network of Isotopes in Precipitation (GNIP, AIEA). Winter: December-February; Spring: March-Mai; Summer: June-August; Fall: September-November. The black cross is the average in precipitation weighted by the volume of precipitation.

(narrow) range of $^{3}H/^{3}He$ ages (Table 1).

In addition, the slightly depleted $^{3}He/^{4}He$ ratio ($R/R_a = 0.97$, Table 2) of the shallow passive sample could be caused by (i) non-equilibrium diffusive gas loss, where the lighter ^{3}He is preferentially lost due to a slightly higher diffusion coefficient compared to ^{4}He (Nakata et al., 2019) or (ii) a contribution of a significant amount of radiogenic ^{4}He. The latter would require either an external influx of He from deeper formations (Torgersen et al., 2013) or outgassing of He from the aquifer solids (Solomon, Hunt and Poreda, 1996). In-situ production by the radioactive decay of uranium and thorium naturally present in the aquifer rock would result in a ^{4}He accumulation rate of $\sim 2.9 \times 10^{-12}$ cc/g/yr (assuming U = 2 ppm and Th = 10 ppm, Heier, 1965). An accumulation time of >3000 years would then be required to explain a R/R_a of ~0.97. This is unlikely regarding the large conductivity and flow velocity of the aquifer (Gobat and Böhi, 2016). Since the origin of the slightly depleted R/R_a value remains unclear, no correction was applied for the shallow passive sample at 9 m.

^{85}Kr piston flow model ages were calculated by resolving the convolution integral (Equation (1)) and using the mean annual ^{85}Kr input curve for Freiburg i.B., Germany (Fig. 2). $^{3}H/^{3}He$ ages were calculated by Equation (7)

$$\tau = \frac{T_{1/2}}{\lambda} \cdot ln\left(1 + \frac{^{3}He_{trit}}{^{3}H}\right) \tag{7}$$

^{85}Kr and $^{3}H/^{3}He$ ages are plotted in Fig. 9 as function of depth below the surface. A good agreement is observed between ^{85}Kr ages and $^{3}H/^{3}He$ ages sampled with the conventional method for the 9 and 15 m levels while the $^{3}H/^{3}He$ ages are shifted towards older values for the deepest level.

The relationship between $\delta^{18}O$ and $\delta^{2}H$ (Table 3) is shown in Fig. 10 and compared with local precipitation and Aare river values. All samples lay on the local precipitation line and are isotopically lighter than the annual mean precipitation value, indicating that recharge occurs predominately in the cooler season (Jasechko et al., 2014). The values from different depth intervals agree within uncertainties. The April samples have a heavier signature, characteristic for warmer temperatures, while the December samples are more depleted indicating recharge under cooler conditions.

3.4. Discussion

The age stratigraphy of groundwater in a homogeneous unconfined aquifer with temporally and spatially constant recharge rate is described by the Vogel model (Vogel, 1967). Equation (8) expresses the age of groundwater at depth z [m], defined as the time since the parcel entered the saturated zone, in an unconfined aquifer with a constant thickness (Cook and Böhlke, 2000). E [m] is the aquifer thickness, φ [-] is the porosity, and R [m/yr] is the recharge rate.

$$t(z) = \frac{E \cdot \varphi}{R} ln\left(\frac{E}{E - z}\right) \tag{8}$$

Assuming realistic values for our study location: a 50 m thick aquifer, a recharge rate of 400 mm/years and a porosity of 20% (Gobat, 2015) results in an age profile which is in reasonable agreement with our tracer ages (Fig. 9).

Potential river water infiltration from the Hagneck channel, as suggested by Gobat and Böhi (2016) and Baillieux et al. (2014), seems to have only a minor effect on the vertical age distribution at the borehole location. However, there are differences and deviations between the individual tracers and the calculated profile that deserve further discussion. One intriguing observation is the systematic shift of ^{85}Kr activities between the passive and the active (conventional) sampling, with lower values for the passive sampling. It is very unlikely that this is related to analytical artefacts or contamination since the conventional method is well established and has been proven contamination free. The lower ^{85}Kr values, and thus older ages, of the passive samples must therefore have an hydrological meaning, which is related to the different sampling regimes. Possible effects to be considered are listed in the following.

First, active pumping from a borehole section drains preferentially water from the most permeable layers. In consequence, the age information from a pumped groundwater sample tends to be biased towards the most active or permeable flow compartments (flow averaged age). In contrast, passive sampling leaves more time for equilibration between the active flow zone and less permeable layers. Passive measurements thus represent the mass or volume averaged age of the entire pore space. On a local scale, even an aquifer considered as homogenous represents a stochastic distribution of permeable, and less permeable zones. In our case, silty layers proportion is increasing with depth (Gobat and Böhi, 2016) and the permeability is consequently decreasing. Pumping drains preferentially water from shallow depths whereas the passive measurements are closer to an undisturbed system. For a polluted aquifer, the arrival time of the contaminants would depend on the fast-flowing pathways while the equilibrium bulk concentration would be related to the water mass in both the permeable and stagnant zones.

Another process that needs to be considered is ambient vertical flow in the open borehole induced by a small head gradient with depth. An upwelling flow of older water would explain why the passive ^{85}Kr ages are older than the conventional one. However, this hypothesis is unlikely as there is no screen bellow the deepest interval and thus, there is

no possibility for an upwelling flow in the borehole up to this level. In addition, special care was taken for the positioning of the packers and the samplers in the center of the screen.

Dispersive admixture of water components that recharged during the time of the bomb peak would explain the apparent shift of $^{3}H/^{3}He$ ages towards old values (Fig. 9) because the age of mixtures is biased towards the components with highest total tritium ($^{3}H+^{3}He$) activity. This is evidenced by total tritium values of 25–27 TU at 22 m (Table 1), which exceeds the input of 6–15 TU from local precipitation (Affolter et al., 2020; Gerber et al., 2018) at the time of recharge.

Finally, a broad distribution of groundwater ages also explains the occurrence of variations in stable isotope composition despite a mean residence time of many years. The difference between the values from April and December (Fig. 10) is interpreted as a seasonal signal carried by the youngest fraction of water composing the exponential age distribution (Vogel, 1967). The relative amplitude of the observed variations between both groups compared to the seasonal recharge variability (winter/summer) is 10% for $\delta^{18}O$ and 4% for $\delta^{2}H$.

4. Conclusion

In this study, we first demonstrate the use of new *in-situ* quasi-passive degassing samplers for Krypton-85 groundwater dating. These membrane contactors allow water degassing directly in the well and gas collection at the surface with minimal logistic facilities in the field. The gas diffusion coefficient through the membrane and thus, the median degassing efficiency and the minimal equilibration time were assessed by laboratory experiments. In the field, the gas collection time is about one day in order to provide the 100–200 L of water required for the analysis. However, it also depends on the natural groundwater flow velocity in the borehole. In open boreholes, a common limitation to passive (or quasi-passive) sampling methods is ambient vertical flow (AVF).

The goal of passive sampling is to obtain groundwater samples with minimal disturbance of the natural flow system. In our case study, we demonstrated a general consistency of ^{85}Kr age profiles obtained by active and passive sampling methods. $^{3}H/^{3}He$ ages depict a similar depth systematics than ^{85}Kr but with older ages in the deepest level.

Additionally, this study emphasizes the importance of the choice of sampling and dating method in a multi-screened open borehole. Aquifer heterogeneities on various spatial scales affect the sampling and tracer methods differently. Conventional sampling for radio noble gases (^{85}Kr, ^{39}Ar) implies a larger water volume and pump rate, and these samples are therefore inherently weighted towards the most permeable parts of the aquifer. Thus, ^{85}Kr values collected by the new quasi-passive method show slightly older ages compared to samples collected by active pumping from isolated screen intervals. Completely passive sampling systems, such as $^{3}H/^{3}He$ diffusion samplers, have a high spatial resolution and are consequently very sensitive to small-scale heterogeneities in the aquifer but also to influences induced by borehole drilling and well construction methods. Such effects impacted the passive $^{3}H/^{3}He$ samples collected in our study. Purely passive methods would benefit of a careful borehole characterization before sampling. Our new *in-situ* sampler for ^{85}Kr represents an intermediate resolution with a mixing length of ~1 m that smooths out micro-scale variabilities while minimizing flow perturbation and maintaining the age stratigraphy on the meter-scale. This corresponds to sampling strategies proposed earlier with moderate pump rates, i.e. low flow sampling (Puls and Barcelona, 1996; Wang et al., 2019). The combined use of different sampling and tracer methods that depict the dynamics and age of waters from distinct aquifer compartments with different conductivities are a valuable tool for the calibration of hydrological models that aim to assess and predict for example the vulnerability of a groundwater body to contamination.

CRediT authorship contribution statement

Stéphanie Musy: Writing - original draft, Conceptualization, Methodology, Investigation, Data curation, Visualization. **Guillaume Meyzonnat:** Investigation, Writing - review & editing. **Florent Barbecot:** Conceptualization, Resources, Writing - review & editing. **Daniel Hunkeler:** Resources, Validation, Writing - review & editing. **Jürgen Sültenfuss:** Resources, Validation, Writing - review & editing. **D. Kip Solomon:** Resources, Validation, Writing - review & editing. **Roland Purtschert:** Supervision, Conceptualization, Investigation, Writing - review & editing, Project administration, Funding acquisition.

Declaration of Competing Interest

The authors declare that they have no known competing financial interests or personal relationships that could have appeared to influence the work reported in this paper.

Acknowledgments

This work was supported by the Swiss National Science Foundation (no.200020/172550). The authors are grateful to Kurt Grossenbacher, Roberto Costa and Laurent Marguet from the Universities of Bern and Neuchâtel for their precious technical support in the field and in the laboratory. We acknowledge Julien Gobat for his help understanding the hydrology of the Seeland Aquifer area, and the department for Water and Wastes from the Canton of Bern for their support.

Appendix

A. Membrane degassing

Gas separation by membranes offers a number of benefits over other gas separation technologies. They are simple to use, cost effective and robust. In this study a dense membrane made of polydimethylsiloxane (PDMS): $[O\text{-}Si[CH3]_2]_n$ was used (Dibrov, 2016). The permeability P_i [$cm^2/s/atm$] of a membrane for a specific gas *i* depends on the gas atoms/molecule size and/or the solubility and diffusivity of the gas in the membrane material. P_i is defined as the product of diffusivity [cm^2/s] and solubility [$cm^3_{STP}/cm^3/atm$] (Zhang and Cloud, 2006). The driving force for the gas to pass through the membrane is the difference in partial pressure $\Delta p_i = p_{0,i} - p_{1,i}$ between both sides of the membrane. The gas flow through the membrane, Q_i [cm^3_{STP}/s] can then be described as:

$$Q_i = \Delta p_i \cdot \frac{P_i \cdot A}{l} \tag{A.1}$$

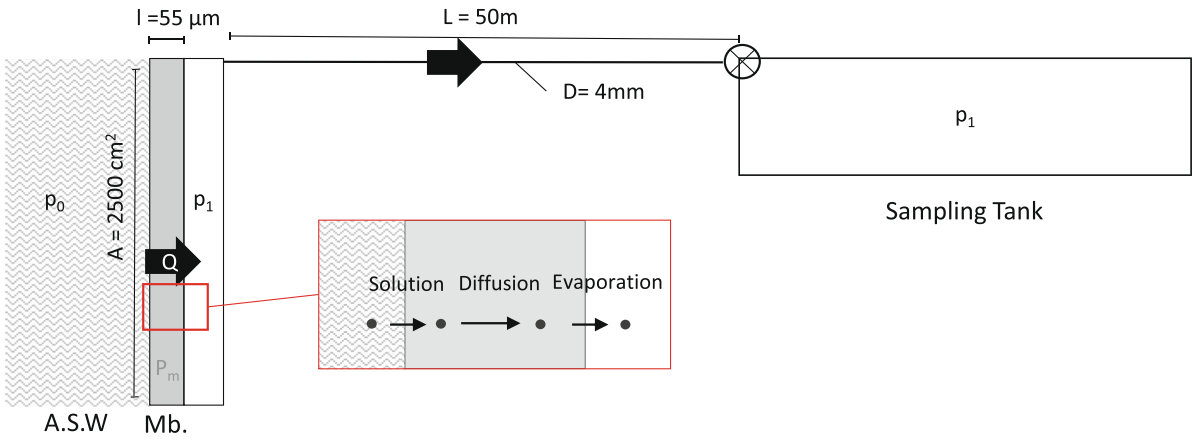

Fig. A.1. Simplified design schematic of a membrane separation process into a sampling tank with volume V. Air equilibrated water (A.E.W) is assumed to be continuously renewed (p_0 = const.). Q is the gas flow through the membrane and trough the tubing. Gas permeation through the membrane is composed of a serial solution-diffusion-evaporation process.

where l [cm] is the membrane thickness, and A [cm^2] is the area of the membrane in contact with water (Fig. A.1)

The temporal pressure increase in the sampling bottle with volume V is then:

$$\frac{\partial p_{1,i}(t)}{\partial t} = Q_i(t)\cdot\frac{P_A}{V} = (p_{0,i} - p_{1,i}(t))\cdot\frac{P_i\cdot A}{l}\cdot\frac{P_A}{V} \tag{A.2}$$

where $P_A = 1atm$. We define then the diffusion parameter for each gas species as $K_i = P_A\cdot P_i \left[\frac{cm^2}{s}\right]$.

Solving the resulting differential Equation (A.2), for each gas species i results in the partial pressure increase as function of time, $p_{1,i}(t)$ (Equation (A.3))

$$p_{1,i}(t) = p_{0,i}\cdot\left(1 - e^{-\frac{K_i\cdot A}{l\cdot V}t}\right) \tag{A.3}$$

The total pressure in the sampling bottle, $p_1(t)$, is then:

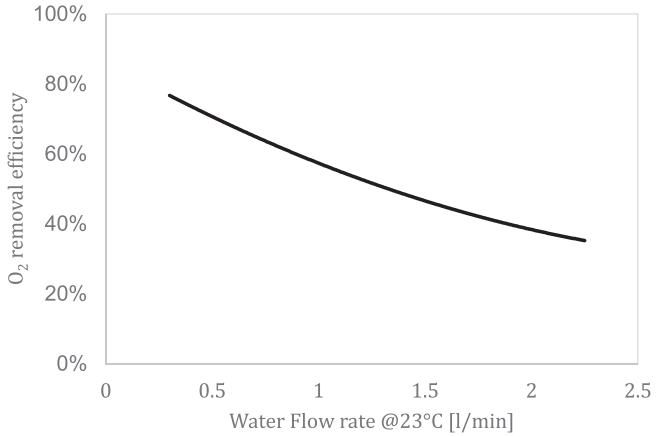

Fig. B.1. Oxygen removal efficiency as function of the water flowrate assuming A.E.W at 10 °C for shell flow and vacuum configuration (Modified from ©Permselect data sheet). Note: slightly different efficiencies for krypton and other gases do not affect the dating results which depend only on the ^{85}Kr/Kr ratio.

$$p_1(t) = \sum_i p_{1,i}(t) = p_0 \left(1 - e^{-\frac{K \cdot A}{l \cdot V} t}\right) \quad \text{(A.4)}$$

where p_0 is the total dissolved gas pressure and K is the total diffusion coefficient for the gas mixture. This equation corresponds to Equation (2). The fractionation that occurs between different gas species i is not affecting the ^{85}Kr dating result because the permeation parameters of ^{85}Kr and ^{84}Kr are almost identical and thus the ^{85}Kr/Kr ratio is maintained.

B. Gas removal efficiency of the membrane contactor used in this study

References

Affolter, S., et al., 2020. Origin and percolation times of Milandre Cave drip water determined by tritium time series and beryllium-7 data from Switzerland. J. Environ. Radioact. 222, 106346 https://doi.org/10.1016/j.jenvrad.2020.106346.

Ahlswede, J., et al., 2013. Update and improvement of the global Krypton-85 emission inventory. J. Environ. Radioact. 115, 34–42. https://doi.org/10.1016/j.jenvrad.2012.07.006.

Ahsan, M., Hussain, A., 2016. Mathematical modelling of membrane gas separation using the finite difference method. Pac. Sci. Rev. A: Nat. Sci. Eng 18 (1), 47–52. https://doi.org/10.1016/j.psra.2016.07.001.

Althaus, R., et al., 2009. Noble gas tracers for characterisation of flow dynamics and origin of groundwater: a case study in Switzerland. J. Hydrol. 370 (1–4), 64–72. https://doi.org/10.1016/j.jhydrol.2009.02.053.

Aoki, N., Makide, Y., 2005. The Concentration of Krypton in the Atmosphere—Its Revision after Half a Century—. Chem. Lett. 34 (10), 1396–1397. https://doi.org/10.1246/cl.2005.1396.

Baillieux, A., et al., 2014. Regional water quality patterns in an alluvial aquifer: direct and indirect influences of rivers. J. Contam. Hydrol. 169, 123–131. https://doi.org/10.1016/j.jconhyd.2014.09.002.

Bethke, C.M., Johnson, T.M., 2008. Groundwater age and groundwater age dating. Annu. Rev. Earth Planet. Sci. 36 (1), 121–152. https://doi.org/10.1146/annurev.earth.36.031207.124210.

Beyerle, U., Aeschbach-Hertig, W., Imboden, D.M., Baur, H., Graf, T., Kipfer, R., 2000. A mass spectrometric system for the analysis of noble gases and tritium from water samples. Environ. Sci. Technol. 34 (10), 2042–2050.

Biaggi, D., et al., 2004 'Hydrogeolgie Seeland Stand 2004'. Grundlagen für Schutz und Bewirtschaftung der Grundwasser des Kantons Bern. / Wasserwirtschaftsamt des Kantons Bern (WWA).

Bollhöfer, A., et al., 2019. Half a century of Krypton-85 activity concentration measured in air over Central Europe: Trends and relevance for dating young groundwater. J. Environ. Radioact. 205–206, 7–16. https://doi.org/10.1016/j.jenvrad.2019.04.014.

Brown, G., 2000. 'The Darcy-Weisbach Equation'. Oklahoma State University–Stillwater. Available at: http://bae.okstate.edu/faculty-sites/Darcy/DarcyWeisbach/Darcy-WeisbachEq.htm.

Cochand, F., et al., 2019. 'Groundwater Model of the Seeland Aquifer'. Bernese Office for Water and Wastes.

Collon, P., Kutschera, W., Lu, Z.-T., 2004. Tracing noble gas radionuclides in the environment. Annu. Rev. Nucl. Part. Sci. 54 (1), 39–67. https://doi.org/10.1146/annurev.nucl.53.041002.110622.

Cook, P.G., Böhlke, J.-K., 2000. 'Determining timescales for groundwater flow and solutes transport', in Environmental Tracers in Subsurface Hydrology. Springer Science+Business Media, LLC. CSIRO Land and Water, Glen Osmond, Australia: Cook Peter G., Herczeg Andrew L., pp. 1–30. Available at: https://link.springer.com/content/pdf/bfm%3A978-1-4615-4557-6/1.pdf.

Cook, P.G., Solomon, D.K., 1997. Recent advances in dating young groundwater: chlorofluorocarbons, 3H3He and 85Kr. J. Hydrol. 191 (1–4), 245–265.

Corcho Alvarado, J.A., Barbecot, F., Purtschert, R., 2009. Ambient vertical flow in long-screen wells: a case study in the Fontainebleau Sands Aquifer (France). Hydrogeol. J. 17 (2), 425–431. https://doi.org/10.1007/s10040-008-0383-1.

Darling, W.G., et al., 2012. The practicalities of using CFCs and SF6 for groundwater dating and tracing. Appl. Geochem. 27 (9), 1688–1697. https://doi.org/10.1016/j.apgeochem.2012.02.005.

Dibrov, G., 2016 'Polydimethylsiloxane Membrane', in Drioli, E. and Giorno, L. (eds) Encyclopedia of Membranes. Berlin, Heidelberg: Springer Berlin Heidelberg, pp. 1–2. 10.1007/978-3-642-40872-4_1401-1.

Gardner, P., Solomon, D.K., 2009. An advanced passive diffusion sampler for the determination of dissolved gas concentrations: passive diffusion samplers. Water Resour. Res. 45 (6) https://doi.org/10.1029/2008WR007399.

Gerber, C., 2012 Development of a New Degassing System for Groundwater Dating with Radio-Noblegases and Application of 85Kr in two Case Studies. Master Thesis. Bern: University of Bern.

Gerber, C., Purtschert, R., Hunkeler, D., Hug, R., Sültenfuss, J., 2018. Using environmental tracers to determine the relative importance of travel times in the unsaturated and saturated zones for the delay of nitrate reduction measures. J. Hydrol. 561, 250–266. https://doi.org/10.1016/j.jhydrol.2018.03.043.

Gobat, J., 2015 Vertikale Schichtung der Grundwasserzusammensetzung im Zuströmbereich der Trinkwasserfassung von Kappelen (BE). Master Thesis. University of Neuchâtel, CHYN Institute.

Gobat, J., Böhi, D., 2016. 'Strengths and weaknesses of groundwater models on the basis of a case study in the Bernese "Seeland"', Swiss bulletin for applied geology 21, 21/1, pp. 53–67.

Harrington, G.A., Cook, E., Robinson, N.I., 2000. Equilibration Times of Gas-Filled Diffusion Samplers in Slow-Moving Ground Water Systems, Groundwater Monitoring and Remediation, 20(2), pp. 60–65.

Heaton, T.H.E., Vogel, J.C., 1981. "Excess air" in groundwater. J. Hydrol. 50, 201–216.

Heier, K.S., 1965. Radioactive elements in the continental crust. Nature 208 (5009), 479–480.

Huber, C., Leuenberger, M., 2005. On-line systems for continuous water and gas isotope ratio measurements†. Isot. Environ. Health Stud. 41 (3), 189–205. https://doi.org/10.1080/10256010500229942.

Jasechko, S., et al., 2014. The pronounced seasonality of global groundwater recharge. Water Resour. Res. 50 (11), 8845–8867. https://doi.org/10.1002/2014WR015809.

Kagabu, M., et al., 2017. Groundwater age determination using 85 Kr and multiple age tracers (SF 6, CFCs, and 3 H) to elucidate regional groundwater flow systems. J. Hydrol.: Reg. Stud. 12, 165–180. https://doi.org/10.1016/j.ejrh.2017.05.003.

Kersting, A., Schlosser, C., Bollhöfer, A., Suckow, A., 2020. Evaluating 5 decades of atmospheric 85Kr measurements in the southern hemisphere to derive an input function for dating water and ice with implications for interhemispheric circulation and the global 85Kr emission inventory. J. Environ. Radioact. 225, 106451. https://doi.org/10.1016/j.jenvrad.2020.106451.

Kozel, R., 1992 Erfassung organischer Spurenbelastungen, insbesondere durch Pflanzenbehandlungsmittel, in oberflächennahen Lockergesteins-Grundwässern. PhD Thesis. University of Neuchâtel, CHYN Institute.

Loosli, H.H., Purtschert, R., 2005. 'Rare gases', in Isotopes in the Water Cycle: Pas, Pressent and Futur of a Developing Science. I.A.E.A, pp. 91–95.

Lu, Z.-T., et al., 2014. Tracer applications of noble gas radionuclides in the geosciences. Earth Sci. Rev. 138, 196–214. https://doi.org/10.1016/j.earscirev.2013.09.002.

Małoszewski, P., Zuber, A., 1982. Determining the turnover time of groundwater systems with the aid of environmental tracers. J. Hydrol. 57 (3–4), 207–231. https://doi.org/10.1016/0022-1694(82)90147-0.

McCallum, J.L., Cook, P.G., Simmons, C.T., 2015. Limitations of the use of environmental tracers to infer groundwater age. Groundwater 53 (S1), 56–70. https://doi.org/10.1111/gwat.12237.

McMillan, L.A., et al., 2014. Influence of vertical flows in wells on groundwater sampling. J. Contam. Hydrol. 169, 50–61. https://doi.org/10.1016/j.jconhyd.2014.05.005.

Meyzonnat, G., et al., 2018. High-resolution wellbore temperature logging combined with a borehole-scale heat budget: conceptual and analytical approaches to characterize hydraulically active fractures and groundwater origin. Geofluids 2018, 20.

Nakata, K., et al., 2019. Degassing behavior of noble gases from groundwater during groundwater sampling. Appl. Geochem. 104, 60–70. https://doi.org/10.1016/j.apgeochem.2019.03.007.

Ohta, T., et al., 2009. Separation of dissolved Kr from a water sample by means of a hollow fiber membrane. J. Hydrol. 376 (1–2), 152–158. https://doi.org/10.1016/j.jhydrol.2009.07.022.

Puls, R., Barcelona, M., 1996. Ground Water Issue: Low-Flow (Minimal Drawdown) Ground-Water Sampling Procedures, p. 12.

Purtschert, R., 2008. 'Timescales and tracers', Natural groundwater quality, pp. 91–108.

Purtschert, R., Yokochi, R., 2013. 'Krypton-81 dating of old groundwater', in Isotope methods for dating old groundwater. I.A.E.A Library. Vienna, pp. 91–124.

Raja Sekhar, G.P., Sano, O., 2000. Viscous flow past a circular/spherical void in porous media – an application to measurement of the velocity of groundwater by the single boring method. J. Phys. Soc. Jpn. 69 (8), 2479–2484. https://doi.org/10.1143/JPSJ.69.2479.

Sanders, D.F., et al., 2013. Energy-efficient polymeric gas separation membranes for a sustainable future: a review. Polymer 54 (18), 4729–4761. https://doi.org/10.1016/j.polymer.2013.05.075.

Singh, B., Chen, J., 2014. Nuclear Data Sheets for A=85. Nucl. Data Sheets 116, 1–162. https://doi.org/10.1016/j.nds.2014.01.001.

Solomon, D.K., Hunt, A., Poreda, R.J., 1996. Source of radiogenic helium 4 in shallow aquifers: Implications for dating young groundwater. Water Resour. Res. 32 (6), 1805–1813. https://doi.org/10.1029/96WR00600.

Suckow, A., 2014. The age of groundwater – definitions, models and why we do not need this term. Appl. Geochem. 50, 222–230. https://doi.org/10.1016/j.apgeochem.2014.04.016.

Sültenfuß, J., Roether, W., Rhein, M., 2009. The Bremen mass spectrometric facility for the measurement of helium isotopes, neon, and tritium in water†. Isot. Environ. Health Stud. 45 (2), 83–95. https://doi.org/10.1080/10256010902871929.

Tomonaga, Y., Marzocchi, R., Pera, S., Pfeifer, H.-R., Kipfer, R., Decrouy, L., Vennemann, T., 2017. Using noble-gas and stable-isotope data to determine groundwater origin and flow regimes: Application to the Ceneri Base Tunnel (Switzerland). J. Hydrol. 545, 395–409. https://doi.org/10.1016/j.jhydrol.2016.11.043.

Torgersen, T., et al., 2013. 'Defining Groundwater Age', in Isotope methods for dating old groundwater. I.A.E.A Library. Vienna, pp. 21–32.

Visser, A., Broers, H.P., Bierkens, M.F.P., 2007. Dating degassed groundwater with 3H/3He. Water Resour. Res. 43 (10) https://doi.org/10.1029/2006WR005847.

Vogel, J.C., 1967. Investigation of groundwater flow with radiocarbon, Isotopes in Hydrology.

Wang, Y., Hou, D., Qi, S., O'Connor, D., Luo, J., 2019. High stress low-flow (HSLF) sampling: a newly proposed groundwater purge and sampling approach. Sci. Total Environ. 6.

White, F.M., 1988. Heat and Mass transfer. Addison-Wesley (Addison-Wesley series in mechanical engineering).

Yokochi, R., 2016. Recent developments on field gas extraction and sample preparation methods for radiokrypton dating of groundwater. J. Hydrol. 540, 368–378. https://doi.org/10.1016/j.jhydrol.2016.06.020.

Zappala, J.C., et al., 2017. Rapid processing of 85Kr/Kr ratios using Atom Trap Trace Analysis. Water Resour. Res. 53 (3), 2553–2558. https://doi.org/10.1002/2016WR020082.

Zhang, H., Cloud, A., 2006. 'The permeability characteristics of silicone rubber', Proceedings of 2006 SAMPE Fall Technical Conference.

Zuber, A., et al., 2011. On some methodological problems in the use of environmental tracers to estimate hydrogeologic parameters and to calibrate flow and transport models. Hydrogeol. J. 19 (1), 53–69. https://doi.org/10.1007/s10040-010-0655-4.